applied sciences

MDPI

Article

Moving Model Experimental Study on a Slipstream of a High-Speed Train Running on the Bridge Suffering a Crosswind

Simin Zou [1,2,3], Xuhui He [1,2,3,*] and Hanfeng Wang [1,2,3,*]

[1] School of Civil Engineering, Central South University, Changsha 410075, China
[2] National Engineering Research Center for High-Speed Railway Construction, Changsha 410075, China
[3] Hunan Provincial Key Laboratory for Disaster Prevention and Mitigation of Rail Transit Engineering Structure, Changsha 410075, China
* Correspondence: xuhuihe@csu.edu.cn (X.H.); wanghf@csu.edu.cn (H.W.)

Abstract: A running train induces a slipstream around it, which is closely related to its aerodynamic features and crucial for the safety of people and structures near the track. However, the effect of crosswinds is almost inevitable when the train runs on a bridge. In this work, an experimental study using moving model testing technology was conducted to investigate the effects of wind speeds, train speeds, and yaw angles on the aerodynamic performance of a Fuxing Hao high-speed train running on a bridge under the influence of crosswind. The results show that, for the crosswind cases, the slipstream velocities on the leeward side of the train are generally higher than those in the no-crosswind cases. Moreover, the results were compared for the cases with the same effective yaw angle of 21.8° but different wind speeds (6 m/s, 8 m/s) and train speeds (15 m/s, 20 m/s), which suggests the method of the resultant wind's yaw angle is no longer valid when the train runs on a bridge due to the aerodynamic interactions.

Keywords: high-speed train; bridge; slipstream; moving model test; crosswind

check for updates

Citation: Zou, S.; He, X.; Wang, H. Moving Model Experimental Study on a Slipstream of a High-Speed Train Running on the Bridge Suffering a Crosswind. *Appl. Sci.* **2023**, *13*, 2521. https://doi.org/10.3390/app13042521

Academic Editor: Giuseppe Lacidogna

Received: 8 January 2023
Revised: 9 February 2023
Accepted: 10 February 2023
Published: 15 February 2023

Copyright: © 2023 by the authors. Licensee MDPI, Basel, Switzerland. This article is an open access article distributed under the terms and conditions of the Creative Commons Attribution (CC BY) license (https://creativecommons.org/licenses/by/4.0/).

1. Introduction

Slipstreams are the flow induced by a moving train, which can cause damage to the infrastructure and destabilize the people near the railway line [1,2]. In recent years, the train-induced slipstream has become a serious safety concern with the spectacular expansion of railway networks and increasing train speeds [3,4]. For example, 16 incidents have been reported in the UK in 32 years since 1972 [5]. More recently, a number of accidents caused by slipstreams were also reported in Switzerland and Austria (two infant fatalities) [6], emphasizing the importance of understanding the slipstream and requirements for a systematic investigation to avoid the induced issues. On the other hand, high-speed trains (HSTs) running on a bridge have become a common scene due to the high bridge ratio in the high-speed railway network. The bridge ratio is usually larger than 50% in the high-speed railway network in China. Particularly, the maximum bridge ratio reaches 94.2% on the Guang-Zhu intercity railway [7].

To study the train-induced slipstream, there are four main methods: full-scale measurement [8–10], the moving model test [11–13], the wind tunnel test [14,15] and numerical simulation [16,17]. Full-scale measurement is an effective way to obtain data from the slipstream of HSTs. Using a full-scale test, Baker et al. [8,9] measured the slipstreams for several different types of passenger trains in Europe to examine their differences and commonalities. Following the experiments in [8,9], Sterling et al. [18] branched out extensive research into a freight train, and the existing network trains' slipstream characteristics were summarized and analyzed. However, a full-scale field test requires a lot of environmental, safety, and cost concerns [19], and the test intervenes too late in the development process of HST-related issues [20].

In recent years, wind tunnel tests and computational simulation are becoming the two approaches widely used to investigate the features of slipstreams [21–23]. Bell et al. [24] investigated the slipstream of high-speed trains in a wind tunnel, and the familiar slipstream characteristics and transient nature of the wake were analyzed. Wang et al. [25] compared the train-induced flow structure and aerodynamic loads for three different ground/wheel configurations by using numerical simulations. Moreover, several other researchers [26–28] have also successfully investigated the slipstream of an HST using wind tunnel tests and computational fluid dynamic (CFD) simulations. Nevertheless, the relative motion between the vehicle and ground/infrastructure is not considered. Furthermore, not only the model used in computational simulations is similar to the wind tunnel tests, but also they require a large number of computing resources and experimental data to validate.

In part because of the paucity of data, the effects of crosswinds on the slipstreams of trains at full scale are poorly understood. Only a few studies have examined the effects of crosswind on the slipstream due to the difficulty in simulating the train running under the crosswind and the unsteady nature of the issue. Investigating how crosswinds affect train slipstreams is challenging to achieve at full scale due to the multivariable ambient winds, as well as the number of trains in operation. The slipstream experienced by an observer may change under crosswinds present under realistic operating conditions. Physical modeling approaches offer controlled environments to conduct experiments, such as wind tunnel testing [29] and moving model testing [30], allowing data to be collected relatively quickly and cheaply compared to full-scale data.

With advances in the technology of the hardware and control methods [31], currently, a moving model test is applicable in studying the HSTs' slipstream and has become more acceptable. It can simulate the relative motion between the train and the ground/infrastructures. Besides, the relationship between crosswind and the train is easier to consider. Using the moving model test method, Baker et al. [32] and Soper et al. [30] investigated the slipstream of a model-scale passenger train ICE2 and freight train Class 66 in the University of Birmingham's Train rig. Subsequently, the ICE3 passenger train was also studied by Bell et al. [11] at DLR-German Aerospace Centre Tunnel Simulation Facility, a moving model facility in Germany.

With the build of China's HSR, the aerodynamic behavior of HST running has aroused more attention [33,34]. With the train's high speed and air viscosity, the airflow around the train develops a special relative unsteady flow, together with the crosswind that makes the mechanism more complicated [35–37]. The work presented aims to analyze the slipstream induced by HST on a bridge under crosswind, including the influence of different train speeds, wind speeds, and yaw angles, highlighting the effect of a bridge and the traditional ways of the method of the resultant wind's yaw angle is not suitable.

2. Experimental Set-Up

2.1. Moving Model Test Rig

To provide insights into the aerodynamic issues of high-speed railways and obtain aerodynamic characteristics of railway-related vehicles and infrastructures, a moving model test rig was developed in the National engineering laboratory for high-speed railway construction at Central South University, Changsha, China [38]. The moving model test rig has a 34 m long double track and consists of three parts: acceleration, test, and deceleration sections. On the other hand, crosswind is one of the prerequisites of exploration, therefore, the moving mode test rig needs a necessary qualification from the crosswind. The wind tunnel of Central South University (CSU) implementation of the strategy for the high-speed railway under crosswind has provided an arena and adequate condition. The moving model test rig spreads over the low-speed test section along both sides of the chamber plotting a moving train & infrastructure system across the wind tunnel. Thus, the moving model test rig can be combined with a wind tunnel to study the high-speed railway aerodynamics under crosswind effects.

As shown in Figure 1, a schematic diagram of the moving model rig, the acceleration and deceleration parts are located on both sides, and the available test part as 12 m long across the wind tunnel's test section. The low-speed section had a dimension of 12 m wide, 3.5 m height, and 18 m long. A 1/16.8 scaled model of a Fuxing HST, which is an HST in operation throughout China, was used in the experiment. The maximum corresponding Reynolds number (Re) of the experimental model was 4.91×10^5, based on the train model height as 0.227 m and train speed U_t. For the present experiments, a constant crosswind can be generated using the wind tunnel during the investigation.

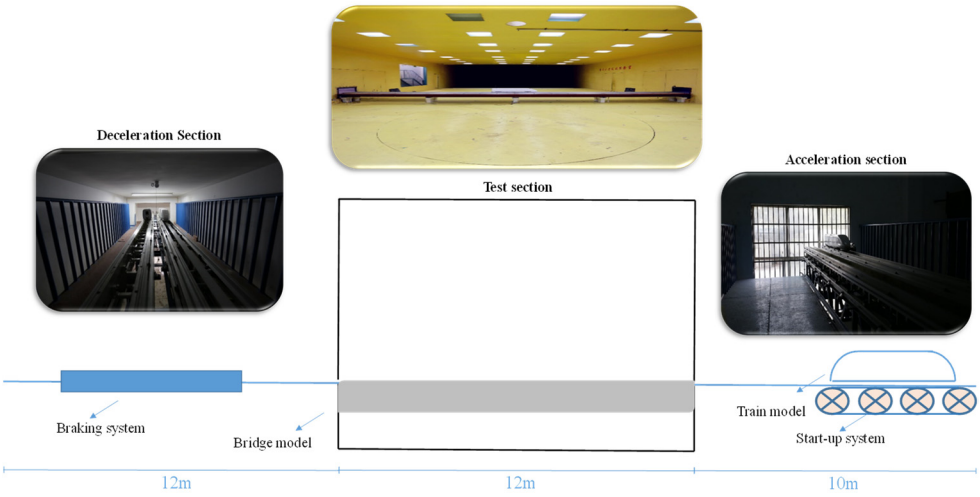


Figure 1. Moving train rig in CSU.

2.2. Slipstream Measurements

To explore the slipstream and flow feature of the present tested model, velocities were measured at a set of monitoring points. For both sides' measurements, a rake of probes located on the leading-edge side of the bridge and the other one on the leeward side of the train. Measurements were taken at full-scale equivalent distances of y = 1.68, 2.18, and 2.69 m from both train lateral surfaces. From there, measuring points would follow the lateral positions mentioned before for the side measurements. Equivalently, considering that z = 0 corresponds to the top of the rail, side measurements along the z-axis were taken at full-scale values of z = 1.21 and 1.55 m. In this way, the slipstream flow property sampling positions are shown in Figure 2 and are used on either side of the train for the windward and leeward samples. The x-axis was defined along the track, the y-axis was the lateral direction, and the z-axis was the vertical direction. x = 0 corresponds to the tip of the train nose. Note that the measurements were conducted at both sides of the train model, to highlight the effects of the crosswind effect. The measurement plane was located at the center of the bridge model along the x direction.

The slipstream velocities during train running on the bridge were obtained and recorded by Cobra probes (Figure 3) and the corresponding signal processing system. The Cobra probe has proved useful in measuring the flow velocity and is frequently used in the studies of the train's slipstreams [39,40]. In the present work, instantaneous velocities within the train-induced slipstream or/and under the influence of crosswind were measured using the Cobra Probe (Turbulent Flow Instrumentation), a four-pressure-hole probe with high-frequency response capable of measuring velocities in three directions [41]. Measurements were conducted at these points one by one. For each point, the sampling frequency of the Cobra probe was 2000 Hz and synchronized with the signal from photoelectric gates, thus the measured velocity could coordinate with the location of the train model.

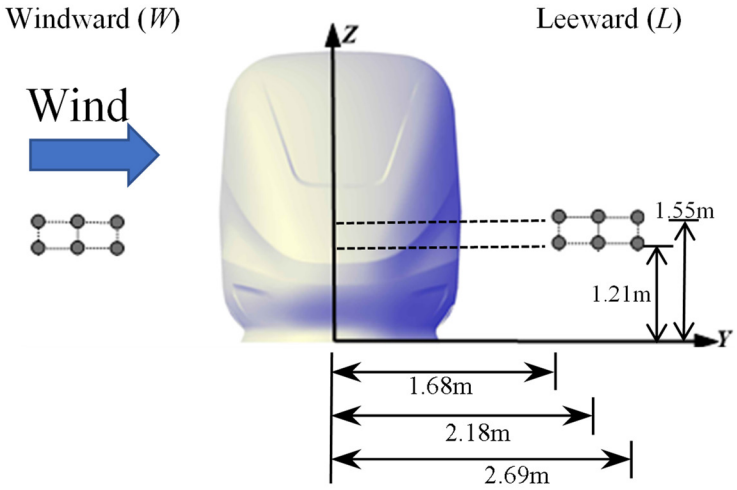


Figure 2. Measurement locations.



Figure 3. 4-hole cobra probe manufactured and calibrated by Turbulent Flow Instruments (http://www.turbulentflow.com.au/ (accessed on 8 February 2023)).

Considering the unstable characteristics of the slipstream, the measured time history of the velocity at a specific position can vary significantly from each run [42]. In the present experiments, following the TSI regulations [43], the measurement at each monitor point was repeated 20 times to get a reliable ensemble-averaged result [44].

Considering some of the unique testing challenges [13] and identifying the crosswind effect on the slipstream, the Cobra probe points to the x-direction during the measurement due to the velocity of the moving train-induced flow being much larger than the crosswind. The measured u, v, and w velocity components correspond to velocities in x-, y-, and z-directions, respectively. Four light gates were used to determine vehicle velocity and acceleration. The vehicle's speed and acceleration were used to convert the measurements from the time domain to the spatial domain, in which all results are presented. Due to the aerodynamics and flow of the head train being particularly sensitive to the influences of crosswind [19,45,46], the main discussion concentrates on the head train. As shown in Table 1, the model section size was 0.227 m × 0.2 m (height × width). The model length was 1.616 m (corresponding to 27.15 m full-scale) with a height ratio L/H of 7.12. The spatial coordinates were also converted into full-scale quantities for easy comparison.

Table 1. Test parameters.

Dimensions of Train	Measurement Locations [1]	Scale Ratio
Length = 27.15 m Width = 3.36 m Height = 3.81 m	y = 1.21 m and 1.55 m z = 1.68 m, 2.18 m, and 2.69 m	1/16.8

[1] y is the distance from the train center, z is the distance from the bridge deck.

2.3. The Source of Crosswind

To investigate details of the interaction and the overlapping of the crosswind and slipstream, hundreds of experiments were carried out with a simulated crosswind provided by the CSU-1 wind tunnel (Central South University, Changsha, China), which is a closed wind tunnel with a reflux mode, essentially consisting of a series of fans with three columns and two rows as shown in Figure 4. The CSU-1 wind tunnel has a reflux mode and consists of two sections: a High-speed section and a Low-speed section that the wind funnels through into the vents in the pipe, blows the test model, and is collected and returned by the return pipe [47]. The wind speed ranges from 0 to 20 m/s, and a good flow quality is adequate for wind engineering and industrial aerodynamic testing with a turbulence intensity level of less than 0.3%.

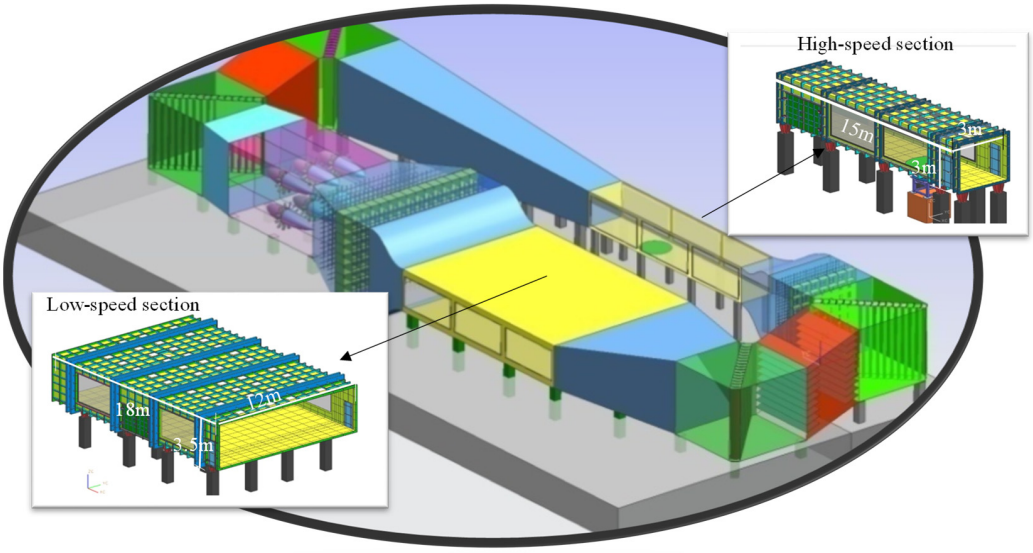


Figure 4. Wind tunnel at Central South University.

3. Slipstream Velocities

3.1. Ensemble-Averaged Velocities

The moving train model test results usually experience substantial variations due to epistemic uncertainties. Ensemble averaging technology is widely used in the process of moving model tests to minimize the uncertainty that provides a smaller relative error in experimental results. In this process, numerous runs were chosen and then converted the time history of velocities to a distance from the passing of the train nose. The same approach has been utilized earlier in studies [11,42].

3.2. Velocity Magnitudes on the Windward Side of the Train

To test the slipstream characteristics of the train running on the bridge under a crosswind, the main measuring points near the train model were selected for testing, and the wind tunnel controlled the crosswind speed during the experiment. See Figure 5 for the variational curve of velocity as the time was measured at z = 1.55 m, y = 1.68, and 2.81 m. Slipstream characteristic tests were carried out under three different conditions: the wind speed (V_w) was 8 m/s with two train speeds (V_t) of 15 and 25 m/s, and a case without crosswind, i.e., the wind tunnel did not open. As shown in Figure 5, the velocity magnitude of the slipstream affected by a crosswind with a speed of 8 m/s was more significant than that under no crosswind, which indicates that crosswinds had a significant impact on the train's slipstream. The peak slipstream velocities were centralized at the nose of the train and values in the no crosswind case were lower than the crosswind in the 8 m/s cases. The flow stagnating on the train nose was still the cause of the peak slipstream velocities. The slipstream velocity in the no crosswind continued to decrease along the train length; however, velocities remained at a higher level influenced by crosswind. Consequently, the

train-induced slipstream velocities are still the main elements in the crosswind cases by comparing results for the same wind speed in different train speeds.

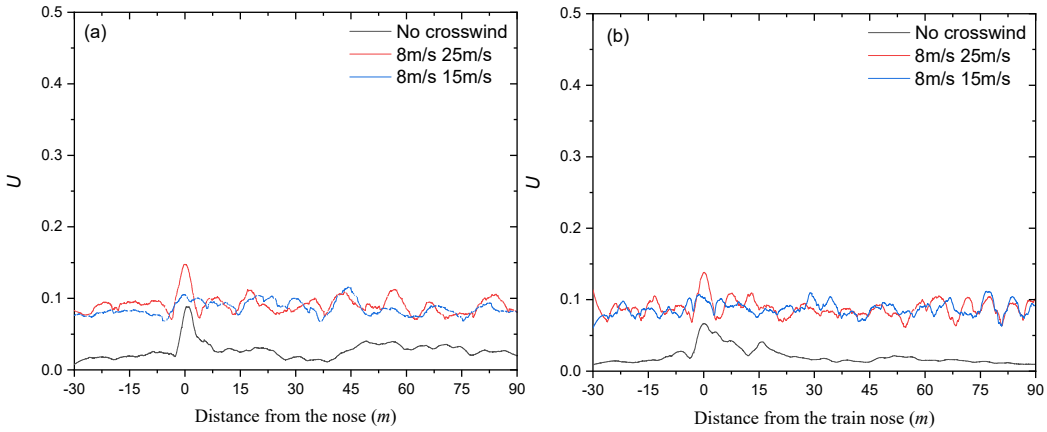


Figure 5. Ensemble−averaged U on the windward side of the train at z = 1.55 m for (**a**) y = 1.68 m, (**b**) y = 2.81 m.

3.3. Velocity Magnitudes on the Leeward Side of the Train

Figure 6 shows the velocity magnitude on the leeward side of the train at z = 1.55 m. On the leeward side, at y = 1.68 m and z = 1.55 m, the nose region velocities of both crosswind cases are within 200% of the no-crosswind peak. With increasing distance from the train side, the difference between the velocities becomes pronounced such that the peak value at the train nose in the three cases is observed to be smaller, and the slipstream velocity in the no crosswind scenario decreased with distance from the train side. In the crosswind cases, the pose variation of slipstream velocities is more complicated and skews are even more distinct for a case of U_w = 8 m/s, U_t = 15 m/s, which indicates that the amplification effects of the crosswinds on the slipstream velocities are more evident on the leeward side of the train and more susceptible to interference from the bridge deck. As the slipstream velocities on the leeward side are more exposed to crosswind and train-induced wind, meaning they suffer ever more direct effects from the crosswind.

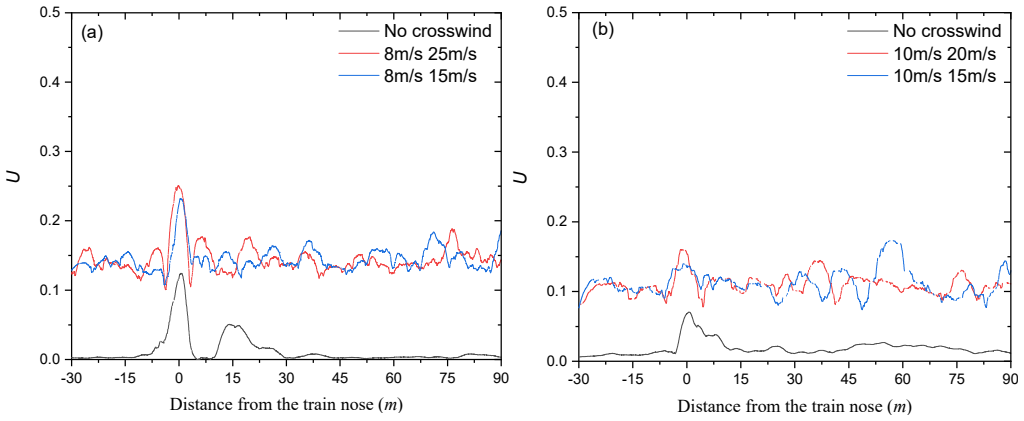


Figure 6. Ensemble−averaged U on the leeward side of the train at z = 1.55 m for (**a**) y = 1.68 m, (**b**) y = 2.81 m.

Generally, the slipstream velocities of both crosswind cases are more significant than the no-crosswind case on the leeward side of the train. This is due to the higher transversal and vertical velocity components in the crosswind cases than in the no-crosswind case. Specifically, the higher velocities from the crosswind cases result from the flow separating around the leeward front corners of the containers and over the roofs causing higher lateral and vertical components compared to the no-crosswind case where the longitudinal component is dominant.

3.4. Effect of Yaw Angle

This is a method widely used when researching the aerodynamics of a train under a crosswind, including the velocity of train-induced slipstream in the presence of a crosswind [41]. The relationship between train-induced slipstream and crosswind velocities is shown in Figure 7; V_w is the crosswind speed, V_t is the train speed vector, and U_{res} is the resultant wind with the resultant yaw angle α (the relative angle between the velocities of the wind and the train).

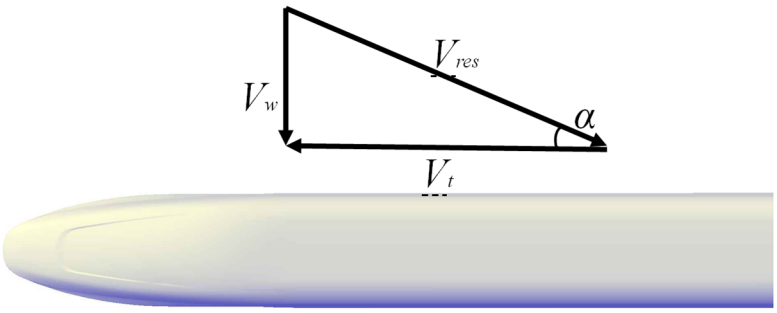


Figure 7. Schematic of the yaw angle of the resultant wind experienced by a moving vehicle in a crosswind.

To investigate the effect of yaw angle flow on the train, the yaw angle was 21.8° depending on the train speed and wind speed, as listed in Table 1, the normalized slipstream velocity magnitude results from both sides of the train U is defined as

$$U = \frac{\sqrt{u^2 + v^2 + w^2}}{u_{res}} \quad (1)$$

where u, v, and w are longitudinal, lateral, and vertical velocity components measured by the Cobra probe, respectively. u_{res} is the relative speed between the train and wind speed.

Ensemble-averaged U from samples at y = 1.68 m, y = 2.25 m, and y = 2.81 m are considered for the no-crosswind and 21.8° crosswind cases with various train speeds and wind speeds. These lateral positions correspond to 0.1 m, 0.6 m, and 1.11 m from the train. The flow variables in the slipstream will be considered at the height of 1.21 m above the surface of the bridge deck.

The U on the windward side of the train for the no-crosswind and 21.8° crosswind cases at z = 1.21 m are shown in Figure 8. In the no-crosswind case, the highest peak velocities are U = 0.173, U = 0.148, and U = 0.08, respectively. The peak U in the no-crosswind case is higher than the crosswind in the 21.8° cases at y = 1.68 m and y = 2.25 m. At y = 2.81 from the train side, the velocity in the no-crosswind and 21.8° cases decreases in the nose region due to the train effect wane. Furthermore, the velocity in the no-crosswind case is lower than in the crosswind cases.

Due to the typical aerodynamic features of a train under the crosswind, the main focus for the aerodynamics of a train has traditionally been the use of the relative yaw angle between the wind speed and train speed. To understand the effect of yaw angle on the slipstream of a train running on the bridge, two cases of Vt = 6 m/s, Vw = 15 m/s, and Vt = 8 m/s, Vw = 20 m/s have been used to compare the slipstream profiles obtained in the same yaw angle. As shown in Figure 8, the slipstream velocities show some similarities in the nose region, boundary layer region, and wake region; especially at y = 1.68 m, the curves of the two 21.8° cases almost overlap. With increasing distance from the train side, the difference between the nose and wake region's velocities becomes more pronounced. These observations indicate that the method using a relative yaw angle may be applicable to the case when the flow is near the train. Once the slipstream is further out of the train, the aerodynamic interference caused by the bridge has significant effects on the slipstream. Thus, the method of relative yaw angle is no longer applicable.

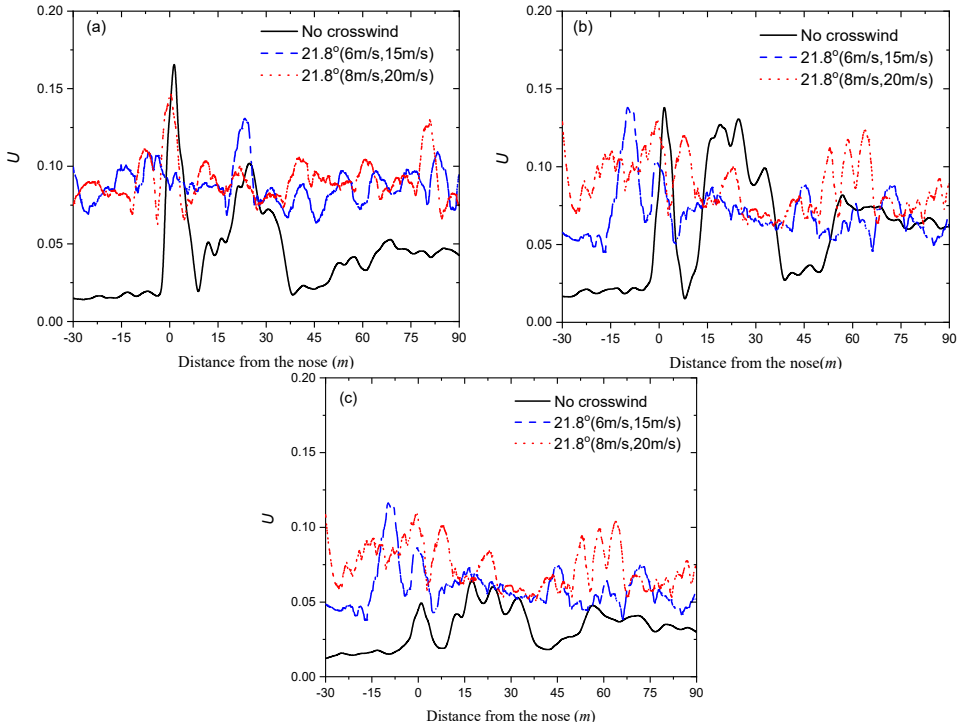


Figure 8. Ensemble−averaged U on the windward side of the train at z = 1.21 m for (**a**) y = 1.68 m, (**b**) y = 2.25 m, (**c**) y = 2.81 m.

Figure 9 shows the U on the leeward side of the train at z = 1.21 m. The nose region velocities of both crosswind cases at y = 1.68 m, y = 2.25, and y = 2.81 m are 15% larger than the no-crosswind peak. At y = 2.25 m, the nose peak of U in 21.8° crosswind cases leaped by more than double the no-crosswind case. With increasing distance from the train, the difference between the velocities in the nose region becomes more pronounced such that the no-crosswind velocity is observed to decrease fastest with distance from the train side, followed by the 21.8° crosswind cases. In the boundary layer region, at y = 2.25 m and y = 2.81 m, the no-crosswind case has the fastest decaying velocity, and the 21.8° cases remain at a high velocity, resulting from the crosswind effect. The larger lateral velocity component causes additional air to pass through the train body, which then accelerates around the leeward tail of the train. This observation is qualitatively analogous to that suggesting the flow is quite three-dimensional along the train when it is running in a crosswind.

For comparison of the two crosswind cases with 21.8° yaw angles, different train speeds and wind speeds are different to the slipstream generation, and the slipstream velocities from the two cases are put in the vast difference. Despite the difference decreasing depending on the distance from the train side increase, the fluctuating range of the external flow curve is higher, and even the flow curve crossover occurs under different train speeds and wind speeds. It seems to reveal the effect of the bridge on the slipstream under the crosswind.

In addition, the slipstream velocities distribution of the moving train varies with different measuring points, predominantly between the different distances from the bridge deck. First, the slipstream velocities from z = 1.55 m measure points at the higher position, indicating that the results of train-induced slipstream stack with crosswind are purer. Due to a shielding effect on the bridge deck on the leading edge, the slipstream velocities from z = 1.21 m have more variability. The higher position from the bridge deck, the fewer interferences from the bridge deck appear to be.

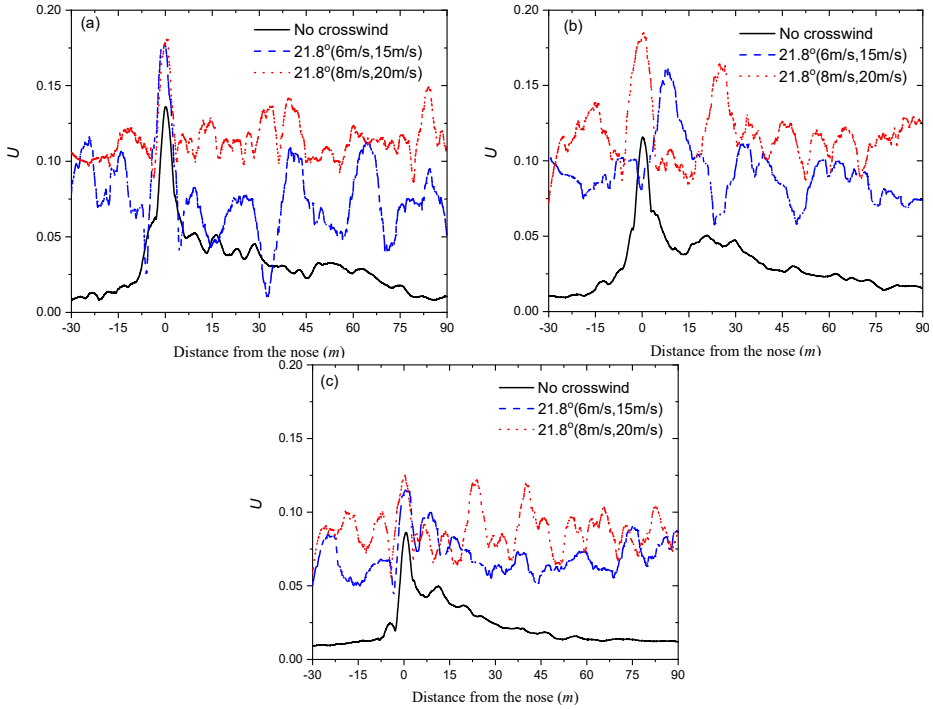


Figure 9. Ensemble−averaged U on the leeward side of the train at z = 1.21 m for (**a**) y = 1.68 m, (**b**) y = 2.25 m, (**c**) y = 2.81 m.

4. Flow Turbulence Intensity

The turbulence intensity of flow around the train is defined as the ratio of the closing velocity (crosswind pass over the train + slipstream) root mean square to the average velocity:

$$I_t = \frac{\sigma_{U'}}{1 - \frac{U'}{u_{res}}} \tag{2}$$

where I_t represents the turbulence intensity, $\sigma_{U'}$ a standard deviation of the normalized slipstream velocity, and U' is the root-mean-square of the turbulent velocity fluctuation.

$$U' = \sqrt{\frac{1}{n}\sum_{1}^{n}[(u_i)^2 + (v_i)^2 + (w_i)^2}} \tag{3}$$

where u_i, v_i, w_i is the instantaneous longitudinal, lateral, and vertical velocity components, respectively, i represent the time step, n is the number of tests, and u_{res} is the closing velocity.

Turbulence intensity (I_t) of the slipstream around the train can be used as a measure of the gustiness of the flow, which is defined as the ratio of the standard deviation of the slipstream velocity ensemble to (1—ensemble mean normalized slipstream velocity) [18]. The results are shown in Figure 10 for two measurement heights. Unsurprisingly, the higher measuring points have the lower turbulence intensity, with the intensities for the z = 1.55 m measurements being significantly less than for the z = 1.21 m measurements. The intensities for turbulence are surprisingly diverse and complex with distance along the train, reflecting that the slipstream was disturbed by the crosswind flow over the bridge deck. For the turbulence intensities on the leeward side, the intensities are much higher as would be expected, with the values for the z = 1.21 m measurements being higher than those for the z = 1.55 m measurements. For both sides of the train, there is considerable variation in intensity along the train. However, it can be seen that the magnitudes of the peaks for the leeward side are significantly greater than for the windward side—for example, the turbulence peaks for the measurements made at 1.21 m height are around 0.21 for the windward side and 0.36 for the leeward side. For the leeward side, the slipstream

will be convected onto the measurement instruments by a crosswind; thus, the results are as expected. I_t on the leeward side is very different from the no-crosswind case [37], suggesting the crosswind has a lasting impact on the turbulence intensity and stacks up the train-induced turbulence to a higher value Relatively higher I_t occurs in the area around the train nose on the leeward side. This is expected because the train-induced flow increases the turbulence generation, thus increasing I_t at a train nose location (Figure 10a). As the flow moves backward along the train, I_t reduces gradually. Remarkably, the I_t in Figure 10a experiences multiple l peaks that disappears in Figure 10b, and the turbulence distribution along the train more chaotic. However, it does suggest there is an influence of the crosswind flows around the bridge and vary between measure points.

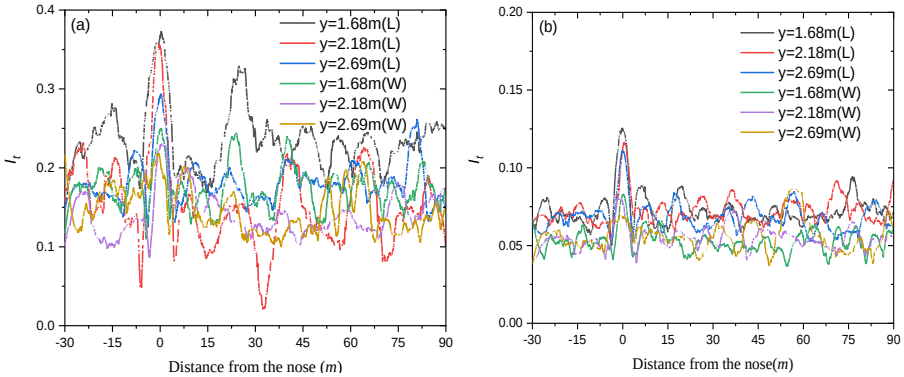


Figure 10. Turbulence intensities at (**a**) z = 1.21 m and (**b**) z = 1.55 m.

5. Conclusions

This paper presented results from a moving model test of slipstream velocities near a high-speed train running on a bridge subjected to crosswinds. From the data presented, the following conclusions are drawn:

The effect of crosswinds on the slipstream essentially increases the measured velocities. Higher velocities were observed on the leeward side of the train in crosswind conditions than on the windward side.

By comparing the effect of the same yaw angle with different train and wind speeds, the method of resultant wind is not applicable when the train runs on a bridge.

The turbulence intensity is relatively higher near the bridge deck and the leeward side. Thus, it suggests an influence of the crosswind flow around the bridge and the turbulence intensity of the slipstream increased by the flow separation and vortex shedding near the bridge.

The CSU moving model test rig has tested the slipstream of the HST running on the bridge. Even though this system obtained the slipstream results of the HST under the crosswind, a more detailed train's aerodynamic characteristic study in a wind environment will be conducted to deepen our understanding of the unsteady behaviors for both train-induced flows, and winds will be further investigated and reported in a future study.

Author Contributions: Conceptualization, S.Z., X.H. and H.W.; methodology, S.Z. and X.H.; writing—original draft preparation, S.Z.; writing—review and editing, H.W.; supervision, X.H. All authors have read and agreed to the published version of the manuscript.

Funding: The study was funded by the National Natural Science Foundations of China (Grant No. 51925808, 52078505), the Tencent Foundation (Xplorer Prize 2021), the Major Special Project (No. 2021-Special-04-02), and the China Postdoctoral Science Foundation (Grants No. 2022TQ0376).

Institutional Review Board Statement: Not applicable.

Informed Consent Statement: Not applicable.

Data Availability Statement: Not applicable.

Conflicts of Interest: The authors declare no conflict of interest.

References

1. Jordan, S.C.; Sterling, M.; Baker, C. Modelling the response of a standing person to the slipstream generated by a passenger train. *Proc. Inst. Mech. Eng. Part F J. Rail Rapid Transit* **2009**, *223*, 567–579. [CrossRef]
2. Liang, X.F.; Zhang, X.; Chen, G.; Li, X.B. Effect of the ballast height on the slipstream and wake flow of high-speed train. *J. Wind. Eng. Ind. Aerodyn.* **2020**, *207*, 104404. [CrossRef]
3. Huang, S.; Hemida, H.; Yang, M. Numerical calculation of the slipstream generated by a CRH2 high-speed train. *Proc. Inst. Mech. Eng. Part F J. Rail Rapid Transit* **2014**, *230*, 103–116. [CrossRef]
4. Meng, S.; Zhou, D.; Xiong, X.; Chen, G. The Effect of the Nose Length on the Aerodynamics of a High-Speed Train Passing Through a Noise Barrier. *Flow Turbul. Combust.* **2022**, *108*, 411–431. [CrossRef]
5. Baker, C.J. A review of train aerodynamics Part 1–Fundamentals. *Aeronaut. J.* **2014**, *118*, 201–228. [CrossRef]
6. Flynn, D.; Hemida, H.; Baker, C. On the effect of crosswinds on the slipstream of a freight train and associated effects. *J. Wind Eng. Ind. Aerodyn.* **2016**, *156*, 14–28. [CrossRef]
7. He, X.H.; Wu, T.; Zou, Y.F.; Chen, Y.F.; Guo, H.; Yu, Z.W. Recent development of high-speed railway bridges in China. *Struct. Infrastruct. Eng.* **2017**, *13*, 1584–1595. [CrossRef]
8. Baker, C.; Quinn, A.; Sima, M.; Hoefener, L.; Licciardello, R. Full-scale measurement and analysis of train slipstreams and wakes: Part 1: Ensemble averages. *Proc. Inst. Mech. Eng. Part F J. Rail Rapid Transp.* **2012**, *98*, 277–298. [CrossRef]
9. Baker, C.; Quinn, A.; Sima, M.; Hoefener, L.; Licciardello, R. Full-scale measurement and analysis of train slipstreams and wakes: Part 2: Gust analysis. *Proc. Inst. Mech. Eng. Part F J. Rail Rapid Transp.* **2012**, *98*, 277–298. [CrossRef]
10. Zampieri, A.; Rocchi, D.; Schito, P.; Somaschini, C. Numerical-experimental analysis of the slipstream produced by a high speed train. *J. Wind. Eng. Ind. Aerodyn.* **2019**, *196*, 104022. [CrossRef]
11. Bell, J.R.; Burton, D.; Thompson, M.; Herbst, A.H.; Sheridan, J. Moving model analysis of the slipstream and wake of a high-speed train. *J. Wind. Eng. Ind. Aerodyn.* **2015**, *136*, 127–137. [CrossRef]
12. Meng, S.; Zhou, D.; Wang, Z. Moving model analysis on the transient pressure and slipstream caused by a metro train passing through a tunnel. *PLoS ONE* **2019**, *14*, e0222151. [CrossRef]
13. Zou, S.; He, X.; Hu, L.; Wang, H.; Kareem, A. Characteristics of the velocity field in slipstream induced by a CR 400 high-speed train lead-carriage. *Measurement* **2022**, *196*, 111205. [CrossRef]
14. Bell, J.R.; Burton, D.; Thompson, M.C.; Herbst, A.H.; Sheridan, J. A wind-tunnel methodology for assessing the slipstream of high-speed trains. *J. Wind. Eng. Ind. Aerodyn.* **2017**, *166*, 1–19. [CrossRef]
15. Jiang, Z.W.; Liu, T.H.; Gu, H.Y.; Guo, Z.J. Research on the reasonable end shape of the windbreak wall model in the wind tunnel test via numerical simulation. *Veh. Syst. Dyn.* **2022**, *60*, 3419–3439. [CrossRef]
16. Wang, X.; Qian, Y.; Chen, Z.; Zhou, X.; Li, H.Q.; Huang, H.L. Numerical studies on aerodynamics of high-speed railway train subjected to strong crosswind. *Adv. Mech. Eng.* **2019**, *11*, 1–12. [CrossRef]
17. Xiong, X.H.; Cong, R.L.; Li, X.B.; Geng, Y.T.; Tang, M.Z.; Zhou, S.J.; Na, Y.L.; Jiang, C.X. Unsteady slipstream of a train passing through a high-speed railway tunnel with a cave. *Transp. Saf. Environ.* **2022**, *4*, tdac032. [CrossRef]
18. Sterling, M.; Baker, C.J.; Jordan, S.C.; Johnson, T. A study of the slipstreams of high-speed passenger trains and freight trains. *Proc. Inst. Mech. Eng. Part F J. Rail Rapid Transit* **2008**, *222*, 177–193. [CrossRef]
19. Zou, S.M.; He, X.H.; Wang, H.F. Numerical investigation on the crosswind effects on a train running on a bridge. *Eng. Appl. Comput. Fluid Mech.* **2020**, *14*, 1458–1471. [CrossRef]
20. Pii, L.; Vanoli, E.; Polidoro, F.; Gautier, S.; Tabbal, A. A full-scale simulation of a high-speed train for slipstream prediction. In Proceedings of the Transport Research Arena, Paris, France, 14–17 April 2014.
21. Hemida, H.; Baker, C.; Gao, G. The calculation of train slipstreams using large-eddy simulation. *Proc. Inst. Mech. Eng. Part F J. Rail Rapid Transit* **2014**, *228*, 25–36. [CrossRef]
22. Bell, J.R.; Burton, D.; Thompson, M.C.; Herbst, A.H.; Sheridan, J. Flow topology and unsteady features of the wake of a generic high-speed train. *J. Fluids Struct.* **2016**, *61*, 168–183. [CrossRef]
23. Wang, S.; Bell, J.R.; Burton, D.; Herbst, A.H.; Sheridan, J.; Thompson, M.C. The performance of different turbulence models (URANS, S.A.S. and D.E.S.) for predicting high-speed train slipstream. *J. Wind. Eng. Ind. Aerodyn.* **2017**, *165*, 46–57. [CrossRef]
24. Bell, J.R.; Burton, D.; Thompson, M.; Herbst, A.; Sheridan, J. Wind tunnel analysis of the slipstream and wake of a high-speed train. *J. Wind. Eng. Ind. Aerodyn.* **2014**, *134*, 122–138. [CrossRef]
25. Wang, S.; Burton, D.; Herbst, A.H.; Sheridan, J.; Thompson, M.C. The effect of the ground condition on high-speed train slipstream. *J. Wind. Eng. Ind. Aerodyn.* **2018**, *172*, 230–243. [CrossRef]
26. Xie, T.Z.; Liu, T.H.; Chen, Z.W.; Chen, X.D.; Li, W.H. Numerical study on the slipstream and trackside pressure induced by trains with different longitudinal section lines. *Proc. Inst. Mech. Eng. Part F J. Rail Rapid Transit* **2018**, *232*, 1671–1685. [CrossRef]
27. Guo, Z.J.; Liu, T.H.; Chen, Z.W.; Xie, T.Z.; Jiang, Z.H. Comparative numerical analysis of the slipstream caused by single and double unit trains. *J. Wind. Eng. Ind. Aerodyn.* **2018**, *172*, 395–408. [CrossRef]
28. Li, W.H.; Liu, T.H.; Martinez-Vazquez, P.; Chen, Z.W.; Huo, X.S.; Liu, D.R.; Xia, Y.T. Correlation tests on train aerodynamics between multiple wind tunnels. *J. Wind. Eng. Ind. Aerodyn.* **2022**, *229*, 105137. [CrossRef]
29. Bell, J.R.; Burton, D.; Thompson, M.; Herbst, A.; Sheridan, J. Dynamics of trailing vortices in the wake of a generic high-speed train. *J. Fluids Struct.* **2016**, *65*, 238–256. [CrossRef]

30. Soper, D.; Baker, C.; Sterliing, M. Experimental investigation of the slipstream development around a container freight train using a moving model facility. *J. Wind. Eng. Ind. Aerodyn.* **2014**, *135*, 105–117. [CrossRef]
31. He, X.H.; Zou, S.M. Advances in wind tunnel experimental investigations of train-bridge systems. *Tunn. Undergr. Space Technol.* **2021**, *118*, 104157. [CrossRef]
32. Baker, C.; Dalley, S.; Johnson, T.; Quinn, A.; Wright, N.G. The slipstream and wake of a high-speed train. *Proc. Inst. Mech. Eng. Part F J. Rail Rapid Transit* **2001**, *215*, 83–99. [CrossRef]
33. Wang, J.B.; Minelli, G.; Dong, T.Y.; He, K.; Krajnovic, S. Impact of the bogies and cavities on the aerodynamic behavior of a high-speed train. An IDDES study. *J. Wind. Eng. Ind. Aerodyn.* **2020**, *207*, 104406. [CrossRef]
34. He, X.; Li, H.; Hu, L.; Wang, H.; Kareem, A. Crosswind aerodynamic characteristics of a stationary interior railway carriage through a long-span truss-girder bridge. *Eng. Struct.* **2020**, *210*, 110350. [CrossRef]
35. Hemida, H.; Krajnovic, S.; Davidson, L. Large-Eddy Simulation of the Flow Around a Simplified High-Speed Train Under the Influence of a Crosswind. In Proceedings of the Aiaa Computational Fluid Dynamics Conference, Toronto, ON, Canada, 6–9 June 2005.
36. Diedrichs, B.; Sima, M.; Orellano, A.; Tengstrand, H. Crosswind stability of a high-speed train on a high embankment. *Proc. Inst. Mech. Eng. Part F J. Rail Rapid Transit* **2007**, *221*, 205–225. [CrossRef]
37. Tian, H.Q. Research progress in railway safety under strong wind conditions in China. *Zhongnan Daxue Xuebao (Ziran Kexue Ban)/J. Cent. South Univ. (Sci. Technol.)* **2010**, *41*, 2435–2443.
38. Zou, S.; He, X.; Wang, H. Moving model experimental analysis of the slipstream produced by a simplistic square-back high-speed train. *Adv. Struct. Eng.* **2022**, *26*, 477–488. [CrossRef]
39. Gil, N.; Baker, C.J.; Roberts, C.; Quinn, A. Passenger Train Slipstream Characterization Using a Rotating Rail Rig. *J. Fluids Eng.* **2010**, *132*, 061401. [CrossRef]
40. Wang, H.F.; Zhou, Y.; Zou, C.; He, X.H. Aerodynamic drag reduction of an Ahmed body based on deflectors. *J. Wind. Eng. Ind. Aerodyn.* **2016**, *148*, 34–44.
41. Chen, J.; Haynes, B.S.; Fletcher, D.F. Cobra probe measurements of mean velocities, Reynolds stresses and higher-order velocity correlations in pipe flow. *Exp. Therm. Fluid Sci.* **2000**, *21*, 206–217. [CrossRef]
42. Baker, C.J. A review of train aerodynamics Part 2–Applications. *Aeronaut. J.* **2014**, *118*, 345–382. [CrossRef]
43. ERA (European Rail Agency). *EU Technical Specification for Interoperability Relating to the Rolling Stock Sub-System of the Trans-European High-Speed Rail System (HS RST TSI), 232/EC*; European Rail Agency: Valenciennes, France, 2008.
44. *CEN EN 140674*; Railway Applications—Aerodynamics. Part 4: Requirements and Test Procedures for Aerodynamics on Open Track. CEN European Standard: Brussels, Belgium, 2013.
45. Copley, J.M. The three-dimensional flow around railway trains. *J. Wind. Eng. Ind. Aerodyn.* **1987**, *26*, 21–52. [CrossRef]
46. Baker, C. The flow around high-speed trains. *J. Wind. Eng. Ind. Aerodyn.* **2012**, *98*, 277–298. [CrossRef]
47. He, X.H.; Zou, S.M. Crosswind effects on a train-bridge system: Wind tunnel tests with a moving vehicle. *Struct. Infrastruct. Eng.* **2021**, *17*, 1–13. [CrossRef]

Disclaimer/Publisher's Note: The statements, opinions and data contained in all publications are solely those of the individual author(s) and contributor(s) and not of MDPI and/or the editor(s). MDPI and/or the editor(s) disclaim responsibility for any injury to people or property resulting from any ideas, methods, instructions or products referred to in the content.